IDENTIFICATION OF ELECTROMAGNETIC SCATTERING MECHANISMS BY TWO DIMENSIONAL WINDOWED FOURIER TRANSFORM APPROACH

A THESIS SUBMITTED TO
THE GRADUATE SCHOOL OF NATURAL AND APPLIED SCIENCES
OF
MIDDLE EAST TECHNICAL UNIVERSITY

BY
K. EGEMEN GERMEÇ

IN PARTIAL FULLFILLMENT OF THE REQUIREMENTS
FOR
THE DEGREE OF MASTER OF SCIENCE
IN
ELECTRICAL AND ELECTRONICS ENGINEERING

DECEMBER 2004

Approval of the Graduate School of Natural and Applied Sciences

Prof. Dr. Canan Özgen
Director

I certify that this thesis satisfies all the requirements as a thesis for the degree of Master of Science.

Prof. Dr. İsmet Erkmen
Head of Department

This is to certify that we have read this thesis and that in our opinion it is fully adequate, in scope and quality, as a thesis for the degree of Master of Science.

Prof. Dr. Mustafa Kuzuoğlu
Supervisor

Examining Committee Members

Prof. Dr. Canan Toker	(METU, EEE)	
Prof. Dr. Kemal Leblebicioğlu	(METU, EEE)	
Prof. Dr. Mustafa Kuzuoğlu	(METU, EEE)	
Assoc. Prof. Gülbin Dural	(METU, EEE)	
Prof. Dr. Adnan Köksal	(HU, EE)	

I hereby declare that all information in this document has been obtained and presented in accordance with academic rules and ethical conduct. I also declare that, as required by these rules and conduct, I have fully cited and referenced all material and results that are not original to this work.

K. Egemen Germeç

ABSTRACT

IDENTIFICATION OF ELECTROMAGNETIC SCATTERING MECHANISMS BY TWO DIMENSIONAL WINDOWED FOURIER TRANSFORM APPROACH

GERMEÇ, Egemen

M.S. Department of Electrical and Electronics Engineering

Supervisor: Prof. Dr. Mustafa Kuzuoğlu

December 2004, 65 pages

In this thesis, it is demonstrated that the two-dimensional Windowed Fourier Transform (WFT) can be effectively used to analyze the local spectral characteristics of electromagnetic scattering signals in the two-dimensional spatial frequency domain. The WFT is the extension of the Short Time Fourier Transform (STFT), which was originally derived to analyze the local spectral characteristics of one dimensional time functions. Since the WFT focuses on the local spectral behavior of the scattered field, the signal localization maps produced in the spectral domain by the WFT can be used to identify the contributions of the rays, at a given location in space, arising from various scattering mechanisms in high frequency applications.

Keywords: Windowed Fourier Transform, Electromagnetic Scattering

ÖZ

ELEKTROMANYETİK SAÇINIM MEKANİZMALARININ İKİ BOYUTLU PENCERELENMİŞ FOURIER DÖNÜŞÜMÜ YÖNTEMİ İLE TANIMLANMASI

GERMEÇ, Egemen

Yüksek Lisans, Elektrik Elektronik Mühendisliği Bölümü

Tez Yöneticisi: Prof. Dr. Mustafa Kuzuoğlu

Aralık 2004, 65 sayfa

Bu tezde, iki boyutlu Pencerelenmiş Fourier Dönüşümü (WFT) yönteminin, iki boyutlu spektral frekans uzayında, elektromanyetik saçınım sinyallerinin lokal spektral karakteristiklerini analiz etmek amacıyla etkili bir şekilde kullanılabileceği gösterildi. Burada kullanılan WFT yöntemi, tek boyutlu ve sadece zamana göre değişen sinyallerin lokal spektral özelliklerini incelemek için geliştirilmiş olan Kısa Zamanlı Fourier Dönüşüm (STFT) yönteminin geliştirilmiş biçimidir. WFT yöntemi saçınım alanlarının lokal spektral davranışlarına odaklandığı için, koordinatları verilen bir uzay noktasına karşılık gelen spektral uzaydaki sinyal yayılma haritaları WFT ile elde edilebilir. Bu haritalar yardımıyla da, yüksek frekans uygulamalarında toplam elektromanyetik saçınım sinyalini oluşturan ve farklı mekanizmalardan kaynaklanan ışınların bireysel katkıları belirlenebilir.

Anahtar Kelimeler: Pencerelenmiş Fourier Dönüşümü, Elektromanyetik Saçınım

To My Family

ACKNOWLEDGMENTS

The author wishes to express his deepest gratitude to his supervisor Prof. Dr. Mustafa Kuzuoğlu for his guidance, advice, criticism, encouragements throughout the research.

TABLE OF CONTENTS

LIST OF FIGURES

FIGURES

CHAPTER 1
INTRODUCTION

1.1 Spatial Signal Analysis in Electromagnetic Scattering

In electromagnetic scattering applications, the scattered field is a vector-valued function of the space coordinate variables. The field variation is a superposition of several components related to the scattering mechanisms introduced by the scattering object. These mechanisms become more pronounced when the scatterer size is much larger than the wavelength. In this case, it is possible to interpret the field variation in terms of ray optics. Therefore, at a certain point in space, it is possible to express the field as a linear combination of rays emanating from the scattering centers of the object [1].

The main aim of this thesis is to identify these rays from the values of the scattered field. These values may be measured or numerically calculated by using the well-known numerical solution techniques. In this thesis, it is demonstrated that the Windowed Fourier Transform (WFT) can be utilized to extract the information related to the ray-optical structure of the field variation.

The WFT provides the means to determine the local field behavior by yielding the approximate plane wave directions. The theoretical basis of this result lies in the representation of electromagnetic field components by plane wave expansions. The validity of this approach is shown via two examples, namely the Sommerfeld half-plane problem, and the scattering of a plane wave by an infinitely long circular perfectly conducting cylinder. In these examples, it has been possible to identify the ray directions by the WFT approach.

1.2 The Windowed Fourier Transform (WFT)

It is well-known that the Fourier transform (FT) $X(\omega)$ of a function $x(t)$ yields the spectral characteristics of that function via the expression

$$X(\omega) = \int_{-\infty}^{\infty} x(t) \exp(-j\omega t) dt \tag{1.1}$$

In several applications, the independent variable t is interpreted as time, and correspondingly ω represents the angular frequency. The Fourier transform of a function is the inner product of $x(t)$ with the complex exponential function $\exp(j\omega t)$, which, when interpreted as a projection in the function space, represents the weight of the function $\exp(j\omega t)$ in the spectral representation of $x(t)$. It is important to note that $x(t)$ is used globally in the expression of the Fourier transform and in order to extract the local spectral information, the Short Time Fourier Transform (STFT) has been introduced [2]. The STFT of a function $x(t)$ is obtained by evaluating the FT of $x(t)$ multiplied by a window function $w(t)$ which slides along the time axis, as shown in (1.2) below:

$$X(t,\omega) = \int_{-\infty}^{\infty} w(t'-t)x(t') \exp(-j\omega t') dt' \tag{1.2}$$

The window function $w(t)$ is a function which is non-zero over a finite duration and the time localization of the function $x(t)$ is achieved by the product $w(t'-t)x(t')$. It is clear that the STFT of $x(t)$ is the Fourier transform of $w(t'-t)x(t')$.

The STFT is a well-known example of a class of signal processing approaches known as time-frequency representations. However, there are several applications where the independent variable is not time. For instance, the independent variable may be one of the space coordinates for representing spatial variations of a quantity. In this case, the term STFT is replaced by the Windowed Fourier Transform (WFT), which yields the local spectral characteristics of a function whose independent variable is not time in general. If the independent variable is a space coordinate, the WFT is a representation yielding the space vs. spatial frequency variation of that function.

The higher dimensional versions of the WFT may be used in the analysis of functions representing spatial variations in two- or three-dimensional space. In this thesis, the WFT is used to analyze the electromagnetic field variations in scattering applications, for the identification of the local ray directions. This information is closely related to the geometric properties of the scatterer, and ray directions may be used to identify the scattering centers (i.e. those points from which the rays emanate) [3-5].

1.3 Outline of This Thesis

The first chapter of this thesis contains the introductory information related to the thesis work. The theoretical analysis related to scattered field calculations and the WFT is given in the second chapter. The examples validating the theoretical work are demonstrated in the third chapter. Finally, the fourth chapter is devoted to the conclusions.

CHAPTER 2
THEORY

2.1 Windowed Fourier Transform (WFT)

2.1.1 Time-Frequency Signal Representations

In real-time signal analysis, the Fourier transform is one of most widely used signal-analysis tool [6]. The basic idea behind the Fourier transform is that any arbitrary signal can be expressed as a superposition of weighted sinusoidal functions. Since its value at a particular frequency is a measure of the similarity of the signal to the sinusoidal basis at that frequency, the frequency attributes of the signal are exactly described.

While the Fourier transform is a very useful concept, the Fourier transform does not explicitly indicate how the frequency content of a signal evolves in time, since the sinusoidal basis functions spread into the entire time domain and are not concentrated in time.

Many signals, mostly the non-stationary signals, encountered in real world situations have frequency content that changes over time. Because of the need to represent this particular nature of the signal, joint time-frequency transforms have been developed that reflects the behavior of the time-varying frequency content of the signal [7].

The spectrum, obtained from the Fourier transform technique, allows us to determine the frequency components that exist for the whole duration of the signal but a joint time-frequency analysis allows us to determine the frequency components at a particular time, so that the frequencies of the dominant sinusoidal components can be displayed at each time instant.

A natural way of characterizing a signal simultaneously in time and frequency domains, based on the expansion and inner product concepts, is to compare elementary functions that are concentrated in both time and frequency domains with the signal.

2.1.1.1 Time Analysis

Time analysis is the investigation of the properties of time-varying quantities. Fundamental physical quantities, such as electric and magnetic fields, change as a function of time and one can call these functions of time as signals, or time waveforms, denoted by the symbol $x(t)$.

Time analysis techniques provide the information related to the time variation of that particular quantity, such as its magnitude at specific time instants, its rate of change with respect to time, its duration, …etc. In order to obtain further information about the signal, it is essential to study the signal in terms of a different representation. A powerful approach in this direction is the spectral representation, which is called frequency analysis.

2.1.1.2 Frequency Analysis

In order to extract further information about a signal, frequency analysis or spectral analysis, is a major requirement. Frequency analysis provides the information related to the frequency content of a signal via the Fourier transform.

2.1.1.3 Linear Time-Frequency Representations (TFRs)

In many signal processing applications, separate time and frequency analysis approaches may not be sufficient. In these cases, it may be useful to combine these two methods to yield the Time-Frequency Representations (TFRs). For any function $x(t)$, a corresponding TFR $T_x(t,f)$ may be obtained, which basically is a representation of the spectral behavior of that signal localized at t.

An important subset of TFRs is a group of representations known as linear TFRs. Linear TFRs satisfy the superposition or linearity principle which states that if $x(t)$ is a linear combination of some signal components, then the TFR of $x(t)$ is the same linear combination of the TFRs of individual signal components by the same weights.

$$x(t) = c_1 x_1(t) + c_2 x_2(t) \Rightarrow T_x(t,f) = c_1 T_{x_1}(t,f) + c_2 T_{x_2}(t,f) \qquad (2.1)$$

Linearity is a desirable property in many applications involving multi-component signals, especially when the isolation of the signal components is needed. The Short-time Fourier Transform is the mostly used linear TFR used to study non-stationary signals [8].

2.1.2 The Short-Time Fourier Transform (STFT)

The Fourier Transform does not give any information on the time interval over which a particular frequency component exists. It does not explicitly reflect the time-varying nature of a signal. It only indicates the presence of various frequency components within the signal, since the basis functions used in the classical Fourier analysis cannot be associated with any particular time instant.

The motivation behind the Short-Time Fourier Transform (STFT) is to obtain the frequency content at a particular time. To this end, the signal is localized around that time instant and Fourier analysis is carried out over this localized signal, neglecting the rest of the signal. Since the time interval which is the support of the localized signal is short compared to the whole signal, this process is called Short-Time Fourier Transform.

The STFT is a formulation that can represent signals of arbitrary duration by breaking them into sub-signals of shorter durations, and applying the FT to each sub-signal. It is based upon a series of overlapped and segmented Fourier transforms that occur across the data stream. In the STFT, the individual Fourier transforms from these multiple segments give a good indication of the time-frequency properties of the signal.

The STFT of a signal $x(t)$ is defined as [9],

$$X_{STFT}^{(w)}(t,f) = \int_{-\infty}^{\infty} x(t')w(t'-t)\exp(-j2\pi f t')dt' \qquad (2.2)$$

where $x(t)$ is a time signal and $w(t)$ is a suitably chosen window function.

The function $w(t)$ could be simply a rectangular pulse of finite duration, although often a Gaussian or Hamming function is used in order to get rid of the undesired effects of the Gibbs phenomenon [10]. The window function simply limits the duration over which the Fourier Transform occurs. This window is then translated along the time axis. By moving $w(t)$ and repeating the same process, one could obtain an idea about the evolution of the frequency contents of the signal.

2.1.2.1 Time-Dependent And Window-Dependent Uncertainty Principle [6]

The time-bandwidth product theorem, or Heisenberg uncertainty principle, has played a prominent role in discussions of joint time-frequency analysis. According to this principle, the product of time and frequency resolution is always greater than a minimum value. The uncertainty principle for the short-time Fourier transform is a function of time, the signal, and the window. Since the uncertainty principle prohibits the existence of windows with arbitrarily small duration and arbitrarily small bandwidth, the joint time-frequency resolution of the short time Fourier transform is inherently limited.

From the original signal $x(t)$, one defines a short duration signal around the time of interest t by multiplying it by a window function that is peaked around the time t and falls off rapidly. This has the effect of emphasizing the signal at time t and suppressing it for times far away from that time.

The choice of a window function indicates both the time and the frequency resolution for the entire representation. Since there is an inherent trade-off between time and frequency localization in short time Fourier transform for a particular window, the window function cannot be chosen arbitrarily. The degree of trade-off depends on the window, signal, time, and frequency.

To summarize, in STFT applications, narrow window means good time resolution but poor frequency resolution and wide window means poor time resolution but good frequency resolution. For a given window, time and frequency resolution of STFT is fixed.

2.1.2.2 Analysis Window Selection

Since the choice of the analysis window directly affects the trade-off between frequency resolution and time resolution as well as the side-lobe attenuation, one has to know the effect of the window.

Let us examine such effects based on a complex exponential signal given in discrete time domain as

$$x(n) = Ae^{jw_0 n} \tag{2.3}$$

If one multiplies this signal with a window function $w(n)$ and takes the discrete time Fourier transform of the resulting product, one obtains the result stated below:

$$X_W(w) = \sum_n x(n)w(n).e^{-jwn} \tag{2.4}$$

$$= A\sum_n w(n).e^{-j(w-w_0)n} \tag{2.5}$$

$$= AW(w - w_0) \tag{2.6}$$

where $W(w)$ is the discrete-time Fourier transform of the window.

So, the transform of a windowed sinusoid is equal to the transform of the window function shifted by an amount equal to the frequency of the sinusoid.

2.1.2.3 An Example for One Dimensional STFT

In the following example, we use a Hamming window but other windows can also be used. Once we have decided on a window function and a window length, we can compute the DFT of this frame. The number of samples of DFT should at least be equal to the window length, with any additional samples being produced via zero padding. The details of the STFT approach are demonstrated in the example given below, based on a joint time-frequency signal representation.

Consider a time domain signal $x(t)$, which is plotted in Figure 2.1, consisting of sinusoids with two different frequencies, the first one with a frequency $\mathrm{f}_1 = 50Hz$ existing over an interval $\mathrm{T}_1 = [1,128]$ seconds, and the second one with a frequency $\mathrm{f}_2 = 100Hz$ existing over the interval $\mathrm{T}_2 = [129,256]$ seconds. The Fourier transform of $x(t)$ is computed and presented in Figure 2.2. It is clearly seen that the plot for the magnitude of the FT indicates the presence of two distinct frequency components of frequencies f_1 and f_2. But it does not give any information about the time range over which a specific frequency component exists.

$$x(t) = \begin{cases} \exp(2j\pi.f_1.x) & 1 \le t \le 128 \\ \exp(2j\pi.f_2.x) & 129 \le t \le 256 \end{cases} \qquad (2.7)$$

One approach, which can give information on the time localization of the spectrum, is the short-time Fourier transform.

In this example, STFT is computed using a MATLAB code, and the magnitude of the STFT output is plotted in Figure 2.3.

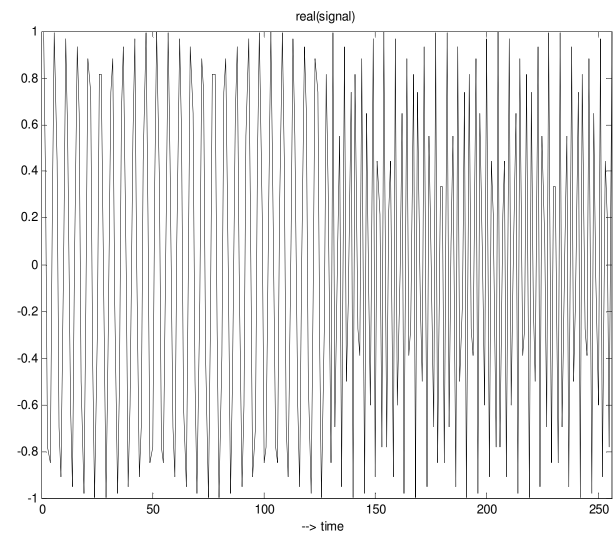

Figure 2.1 Time characteristic of the signal (Real part of the signal).

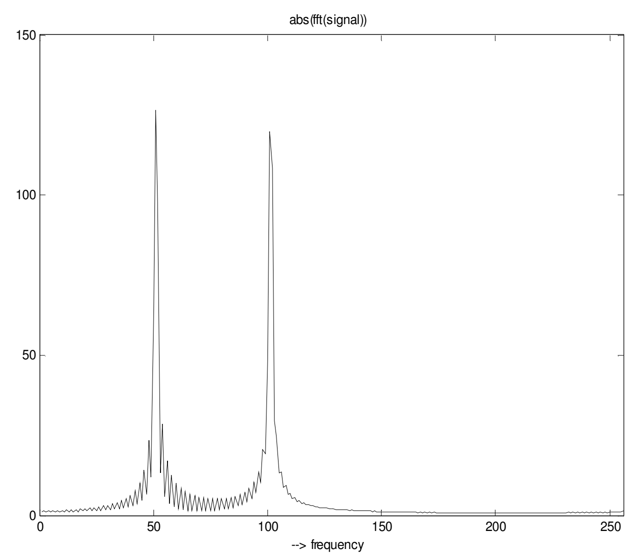

Figure 2.2 Frequency characteristic of the signal (Magnitude of FFT of the signal).

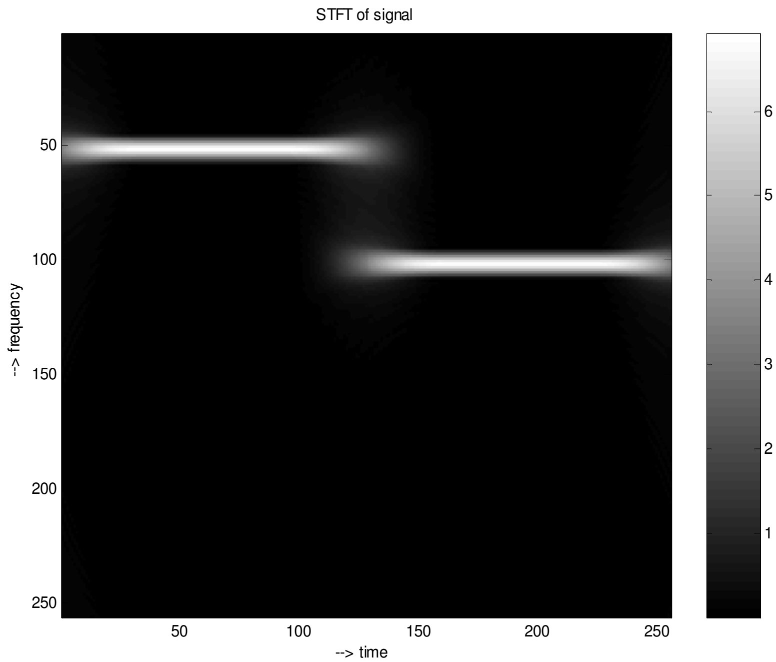

Figure 2.3 Time-frequency characteristics of the signal (Magnitude of STFT of signal).

By using the STFT approach, we can see that, two different time-frequency components can be clearly located. It gives information about when these different frequencies f_1 and f_2 occur or how they change over time.

If the window is too wide, we get good frequency resolution, but we lose the information of any locality, and if the stationary part of the signal is shorter than the window width, the results start to become useless. If the window is shorter than the stationary part of the signal, the frequency information that was important is lost, at the expense of knowing when it occurred.

2.1.2.4 Space-Spatial Frequency Distributions

In some applications, the signal to be analyzed may be a function of one or more space variables. Then, in contrast to the conventional frequency concept used in the spectral analysis of time signals, the variables in the Fourier transform will be spatial frequencies. In this case, the STFT approach is replaced by the WFT as explained below.

2.1.3 The Windowed Fourier Transform (WFT)

To extract local-frequency information from a signal (the independent variable may be time, space coordinate, …etc.) , the Windowed Fourier Transform represents an analysis technique. The approach is identical to the STFT in the sense that a sliding window function is used in the FT to obtain the local spectral properties.

2.1.3.1 Shannon Sampling Theorem and Nyquist Sampling Rate

According to the Shannon sampling theorem, it is possible to reconstruct a function exactly from its samples, provided that the function is band-limited and the sampling frequency is sufficiently high to resolve its highest frequency components.

The sampling theorem gives a directive for selecting sufficiently small grid spacing Δx once the band-limit Ω is known. It states that Δx must be chosen to satisfy the critical sampling rate $\Delta X = \frac{1}{\Omega}$ which is called the Nyquist sampling rate and the frequency $\frac{\Omega}{2}$ is known as the Nyquist frequency. The Nyquist frequency is the highest frequency that can be resolved using a given sample spacing Δx and all higher frequencies will be aliased to lower frequencies. The Nyquist sampling rate is the largest grid spacing that can resolve the frequency and this also implies that in order to resolve a single sinusoidal function, one must have at least two sample points per period of the wave.

Assume that f is a band-limited function whose Fourier transform is zero outside of the interval $\left[-\frac{n}{2}, \frac{n}{2}\right]$. If Δx is chosen as:

$$\Delta X < \frac{1}{\Omega}, \tag{2.8}$$

then f may be reconstructed exactly from its samples as follows

$$f_n = f(n\Delta x) = f(x_n) \tag{2.9}$$

$$f(x) = \sum_{n=-\infty}^{\infty} f_n \sin c\left(\frac{\pi(x - x_n)}{\Delta x}\right) = \Delta x \sum_{n=-\infty}^{\infty} f_n \frac{\sin(\pi(x - x_n)/\Delta x)}{\pi(x - x_n)} \tag{2.10}$$

where the *sinc* function is given by $\sin c(x) = \frac{\sin(x)}{x}$, shown in Figure 2.4 below.

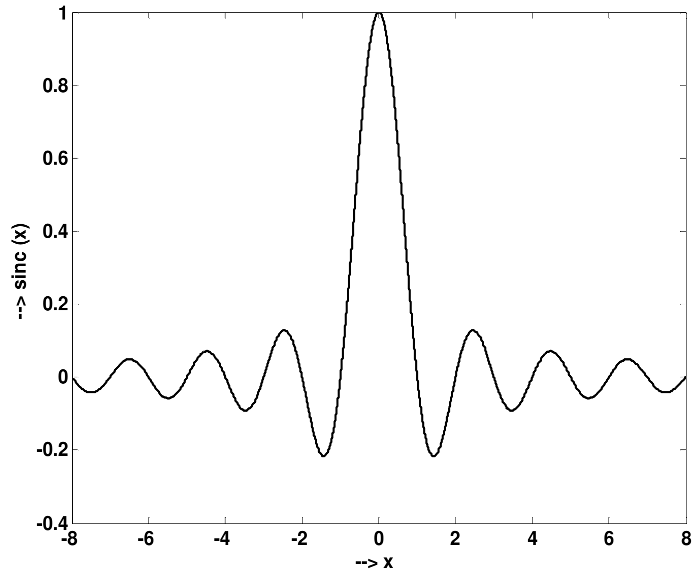

Figure 2.4 The $\sin c$ function $\sin c(x) = \sin c(x)/x$

2.1.3.2 Two Dimensional Windowed Fourier Transform

The two dimensional windowed Fourier transform of a signal $f(x, y)$ is defined by

$$WFT_f(x, y, k_x, k_y) = \int\int f(\alpha, \beta) w(\alpha - x, \beta - y) e^{-(jk_x\alpha + k_y\beta)} d\alpha\, d\beta \quad (2.11)$$

where $w(\alpha, \beta)$ denotes a two-dimensional, usually even and real-valued, window function.

The standard procedures used to realize one dimensional WFT approaches, can be suitably generalized to the two dimensional case as demonstrated in the example below.

2.1.3.3 An Example for the Two Dimensional WFT

Consider a spatial signal, as shown in Figure 2.5, consisting of two localized sinusoids with frequencies (fx_1, fy_1) and (fx_2, fy_2).

The first component has frequency $fx1 = 10(1/m)$ and $fy1 = 0(1/m)$ existing over an interval $x = [0,2]$ meters and $y = [0,2]$ meters (Region 1) and the second a frequency $fx2 = 20(1/m)$ and $fy2 = 0(1/m)$ existing over another interval $x = [-2,0]$ meters and $y = [-2,0]$ (Region 3).

The Fourier Transform gives two approximate 2D *sinc* functions without any implication of localization. Space and frequency characteristics of the signal are different in the regions below:

$\text{Region1}: x > 0 \;\&\; y > 0$

$\text{Region2}: \mathrm{x} < 0 \;\&\; y > 0$

$\text{Region3}: \mathrm{x} < 0 \;\&\; y < 0$

$\text{Region4}: \mathrm{x} > 0 \;\&\; \mathrm{y} < 0$

We simulate this 2D signal, which exists in $x = [-2,+2]$ and $y = [-2,+2]$ with $256\mathrm{x}256$ samples by a Matlab code.

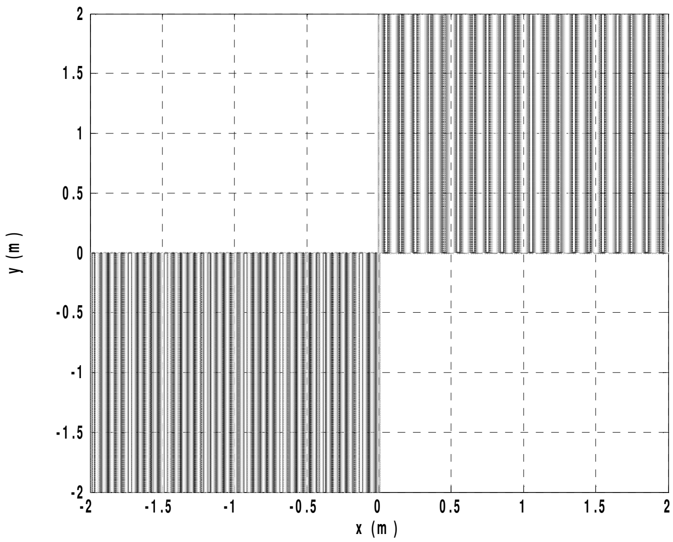

Figure 2.5 Spatial characteristic of the 2D signal (Real part of the signal).

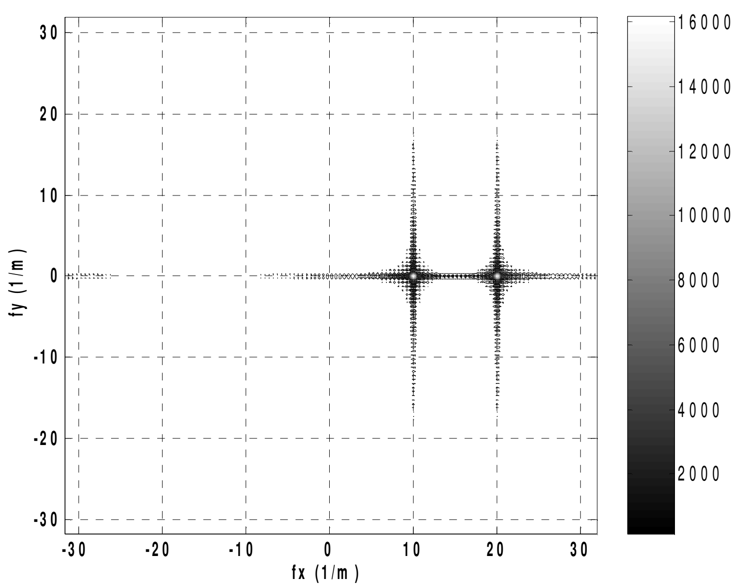

Figure 2.6 Frequency characteristic of 2D signal (Magnitude of FFT of signal).

In this example, we use a Hamming window in the Matlab code, but other windows can possibly be used. Once we have decided on a window function and a length, we can compute the 2D DFT of this frame. The size of this 2D DFT is chosen to be at least window length, with any additional samples being produced via zero padding.

One approach, which can give information on the space resolution of the spectrum, is the 2D WFT. A moving 2D window can be applied to the signal and the Fourier transform is applied to the signal within the window as the window is moved.

In order to have an idea of what can be achieved by the 2D WFT, the following results are obtained. The grid is $256\mathrm{x}256$ and the window function is Hamming with a length occupying 65 samples in x and y.

The 2D WFT is evaluated at $[x = 1.5, y = 1.5]$, which is in the first region, and then at $[x = -1.5, y = -1.5]$ which is in the third region.

When we plot the windowed Fourier Transform at $[x = 1.5, y = 1.5]$ which is in the first region, we can see only the frequency characteristic of the signal focused around (fx_1, fy_1), as shown in Figure 2.7, and when we plot the windowed Fourier Transform around center $[x = -1.5, y = -1.5]$, which is in the second region, we can see only the frequency characteristic of the signal focused around (fx_2, fy_2) as expected, as shown in Figure 2.8.

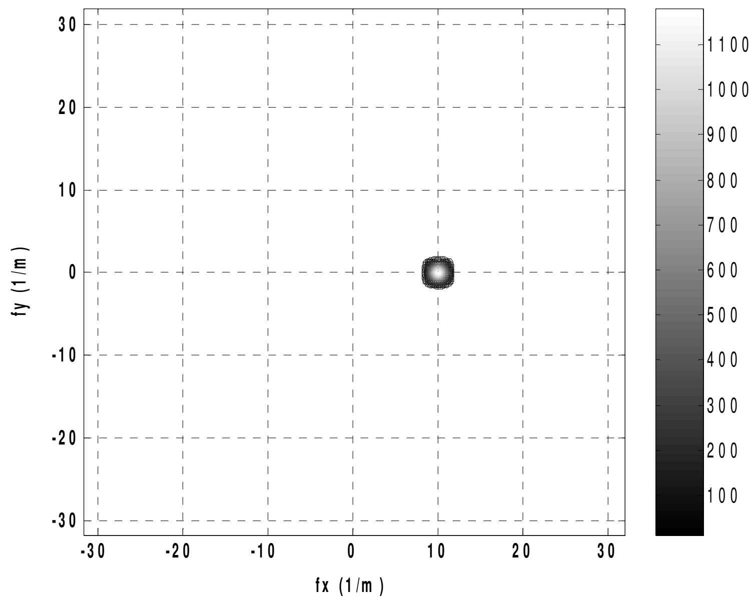

Figure 2.7 Magnitude of 2D WFT of signal around center $x = 1.5, y = 1.5$

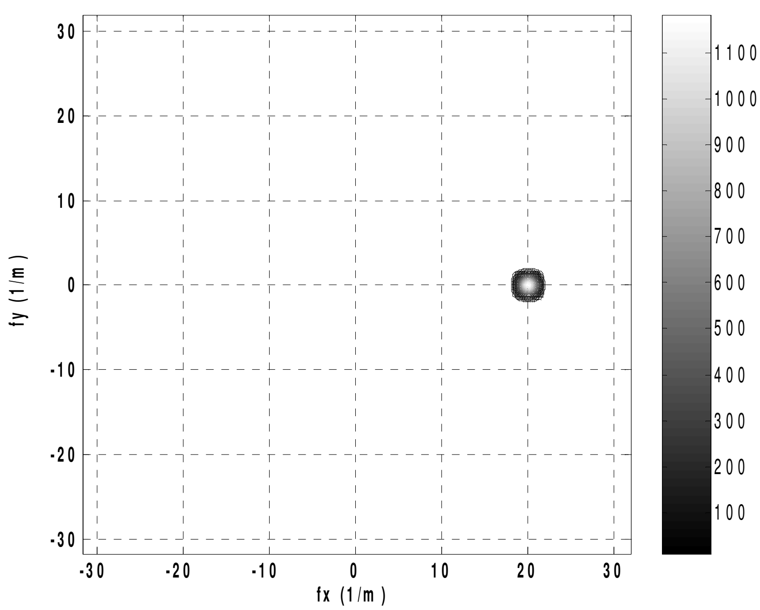

Figure 2.8 Magnitude of 2D WFT of signal around center $x = -1.5, y = -1.5$

As a result, by using the 2D WFT, we can see that the two space-frequency components can be clearly identified, located around the locus of the two frequencies. It gives information about when these different frequencies (fx_1, fy_1) and (fx_2, fy_2), occur or how they change over the spatial domain.

2.2 Electromagnetic Scattering

2.2.1 Introduction

If an electromagnetic wave is incident on an object, which may be perfectly conducting or dielectric, the wave is scattered because of the presence of the object. The sum of the incident and the scattered fields form the total field.

Most of the scattering problems can not be solved exactly due to the complex shape (or material parameter variations) of the scatterer, and approximate numerical approaches are used to analyze scattering problems. The most well-known approaches are

1. Finite Difference Time Domain (FDTD) method [12],
2. Method of Moments (MoM) [13],
3. Finite Element Method (FEM) [14].

Finite Difference Time Domain (FDTD) method is one of the most successful numerical approaches to the direct solution of Maxwell's curl equations governing the electric and magnetic field in time domain.

Method of Moments (MoM) is used to solve a certain class of integro-differential equations to analyze (mostly) perfectly conducting structures.

Finite Element Method (FEM) is commonly used for modeling complex, in-homogenous structures for the solution of the Maxwell's differential equations. In this method the unknown function is approximated on a domain, which is represented by a set of elements of simple shape with a finite number of parameters.

2.2.2 Mathematical Formulation

In scattering problems the incident field is usually taken as a plane wave given by

$$\overline{E}_i(\overline{r}) = \hat{e}_i \exp(-jk\hat{i}.r) \tag{2.12}$$

The amplitude $|E_i|$ is chosen to be 1 (volt/m), $k = w\sqrt{\mu_0 \varepsilon_0} = (2\pi)/\lambda$ is the wave number, λ is a wavelength in the medium, $\hat{i}$ is a unit vector in the direction of wave propagation, and $\hat{e}_i$ is a unit vector in the direction of its polarization [11].

Associated with $\overline{E}_i$, there is a magnetic field $\overline{H}_i$, which is perpendicular to $\overline{E}_i$, given by:

$$\overline{H}_i(\overline{r}) = (\hat{i} \text{x} \hat{e}_i) \exp(-jk\hat{i}.r) \tag{2.13}$$

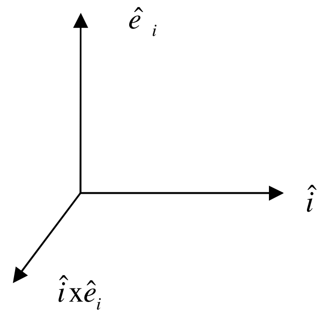

Figure 2.9 Directions of $\overline{E}$ and $\overline{H}$ fields and the propagation.

Both $\overline{E}_i$ and $\overline{H}_i$ satisfy Maxwell's curl equations in free space:

$$\nabla \text{x} \overline{E}_i = -jw\mu_0 \overline{H}_i \tag{2.14.a}$$

$$\nabla \text{x} \overline{H}_i = -jw\mu_0 \overline{E}_i \tag{2.14.b}$$

If $\overline{H}_i$ is eliminated, $\overline{E}_i$ satisfies the homogeneous vector wave equation given by:

$$\nabla \text{x}(\nabla \text{x} \overline{E}_i) - k^2 \overline{E}_i = 0 \tag{2.15}$$

Now, consider a non-magnetic dielectric object with permittivity $\hat{\varepsilon}$ and permeability μ_0, occupying a region Ω in R^3, as shown in Figure 2.10 below.

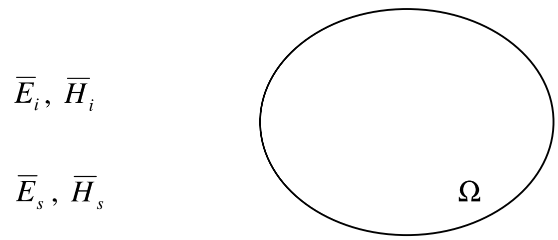

Figure 2.10 A non-magnetic dielectric scatterer with permittivity $\hat{\varepsilon}$ and permeability μ_0, occupying a region Ω in IR^3.

where the incident field components are given by the equations $(2.12-2.13)$ in the absence of the scattering object and $(\overline{E}_s, \overline{H}_s)$ are the scattered field components whose sources are in Ω.

The total field components $(\overline{E}_t, \overline{H}_t)$ are defined as:

$$\overline{E}_t = \overline{E}_i + \overline{E}_s \tag{2.16.a}$$

$$\overline{H}_t = \overline{H}_i + \overline{H}_s \tag{2.16.b}$$

which satisfy:

$$\nabla \mathrm{x} \overline{E}_t = -jw\mu\overline{H}_t \tag{2.17.a}$$

$$\nabla \mathrm{x} \overline{H}_t = -jw\varepsilon \overline{E}_t \tag{2.17.b}$$

where $\mu = \mu_0$ everywhere and $\varepsilon = \varepsilon_0$ outside Ω and $\varepsilon = \hat{\varepsilon}$ within Ω.

After substituting (2.16)in (2.17), the following equations are obtained

$$\nabla \mathrm{x}(\overline{E}_i + \overline{E}_s) = -jw\mu_0(\overline{H}_i + \overline{H}_s) \text{ everywhere} \tag{2.18.a}$$

$$\nabla \mathrm{x}(\overline{H}_i + \overline{H}_s) = jw\varepsilon_0(\overline{E}_i + \overline{E}_s) \text{ outside } \Omega \tag{2.18.b}$$

$$\nabla \mathrm{x}(\overline{H}_i + \overline{H}_s) = jw\hat{\varepsilon}(\overline{E}_i + \overline{E}_s) \text{ inside } \Omega \tag{2.18.c}$$

Using (2.16) and $(2.18a - 2.18b)$, the following equation is generated:

$$\nabla \mathrm{x} \overline{E}_s = -jw\mu_0 \overline{H}_s \tag{2.19.a}$$

$$\nabla \mathrm{x} \overline{H}_s = -jw\varepsilon_0 \overline{E}_s \text{ outside } \Omega \tag{2.19.b}$$

Finally, for the scattered field inside Ω, we obtain

$$\nabla \mathrm{x}\overline{H}_i + \nabla \mathrm{x}\overline{H}_s = jw\hat{\varepsilon}\overline{E}_i + jw\hat{\varepsilon}\overline{E}_s \tag{2.19c}$$

and using (2.13), we obtain:

$$\nabla \mathrm{x}\overline{H}_s = jw(\hat{\varepsilon} - \varepsilon_0)\overline{E}_i + jw\hat{\varepsilon}\overline{E}_s \text{ inside } \Omega \tag{2.19d}$$

The term $jw(\hat{\varepsilon} - \varepsilon_0)\overline{E}_i$ acts as a source term for the scattered field [15].

Equations $(2.19a - 2.19b - 2.19c)$ are the governing partial differential equations of the scattered field. It is noted that outside the scatterer, the equations turn out to be free-space Maxwell's equations, and inside the scatterer, the equation $(2.19d)$ is not homogenous, containing a source term creating the scattered field.

If Ω represents a PEC object, the total field vanishes within Ω and the scattered field satisfies $(2.19a)$and $(2.19b)$. The sources of the scattered field lie on $\partial\Omega$ (representing the boundary of Ω) and they are represented by the boundary condition

$$(\hat{n}\mathrm{x}\overline{E}_s) = -(\hat{n}\mathrm{x}\overline{E}_i) \tag{2.19e}$$

where $\hat{n}$ is the unit outward normal on $\partial\Omega$.

2.2.3 Dependence of the Scattering Characteristics to Object Geometry and Material Properties

The scattering characteristics of an object depend on its geometry (size, shape, etc.) and its material properties ($\varepsilon, \mu,$ and σ). For a PEC object, the scattered field variation is a complicated function of the shape of the scatterer. In addition, for time-harmonic excitations (i.e. when the excitations are sinusoidally varying with an angular frequency ω), the scattered field also exhibits a dependence on the wave number k (which is directly proportional to ω).

The scattering characteristics are determined by comparing the object size with the wavelength of the electromagnetic excitation. The parameter representing the object size is d, which is a dimension characterizing the PEC object. For example, d may represent the side-length for a cube. If $d << \lambda$, the frequency domain calculations are carried out in the low-frequency region, where the magnitude of the scattered field is very small compared to the magnitude of the incident plane wave. The Born and Rytov approximations are used to handle low frequency scattering problems [11].

If $d \approx \lambda$ (i.e. if d is comparable to wavelength λ), the calculations are performed in the resonance region, implying that there is considerable interaction between the object and the electromagnetic excitation.

The high-frequency region $(d >> \lambda)$ is also called the optical region, since the scattering mechanism is similar to the scattering of visible light by objects to be detected by the human eye.

The calculation of the scattered field is not an easy task, because of the complicated dependence of the field variation to the geometry of the scatterer. The analytical solution of scattering problems can be obtained only for a few specific cases. The field scattered by a PEC sphere or an infinite cylinder for plane wave incidence, can be obtained by solving the governing partial differential equations by using separation of variables and the complete solution is obtained in the form of an infinite series [15].

There are other problems such as the Sommerfield half-plane problem, or the edge scattering problem, that can be solved analytically. If the analytical solution is not achievable, one may try to obtain an approximate solution via FEM, MoM or FDTD as explained earlier. In all these methods, the computational domain is discretized (i.e. it is represented as a union of smaller sub-domains) and the unknown function (which is either $\overline{E}$ and $\overline{H}$ field variation, or an equivalent surface or volume current density, $\overline{J}$). Finally, the integral or differential equation is solved approximately, yielding the unknowns. The numerical solution techniques are effective for low or medium frequency range, and for high frequency applications they become formidable, because of the necessity to employ a large number of unknowns to model the problem. For high frequency applications, methods based on ray-optical approaches are quite popular, and the most well-known ray-optical approach is the Geometric Theory of Diffraction (GTD) introduced by Keller [3].

The geometrical theory of diffraction is an extension of geometrical optics, which accounts for diffraction. It introduces diffracted rays in addition to the usual rays of geometrical optics. These rays are produced by incident rays which hit edges, corners, or vertices of boundary surfaces or which graze such surfaces.

Various laws of diffraction, analogous to the laws of reflection and refraction, are employed to characterize the diffracted rays. A modified form of Fermat's principle, equivalent to these laws, can also be used. Diffracted wave fronts are defined, which can be found by a Huygens wavelet construction. There is an associated phase or eikonal function, which satisfies the eikonal equation. In addition, complex or imaginary rays are introduced. A field is associated with each ray and the total field at a point is the sum of the fields on all rays through the point. The phase of the field on a ray is proportional to the optical length of the ray from some reference point. The amplitude varies in accordance with the principle of conservation of energy in a narrow tube of rays. The initial value of the field on a diffracted ray is determined from the incident field with the aid of an appropriate diffraction coefficient. These diffraction coefficients are determined from certain canonical problems. They all vanish, as the wavelength tends to zero.

2.2.4 Examples of Scattering Applications

In this section, two scattering problems will be studied, namely i) the scattering of a TM_z plane wave by an infinite PEC circular cylinder whose axis is paralled to the z-axis, and ii) the Sommerfeld half-plane problem. In both cases, the ray optical approach will be underlined, since our ultimate aim is to identify the ray directions by the 2D WFT.

2.2.4.1 The Circular Cylinder Scattering Problem

Consider the diffraction of a plane electromagnetic wave by an infinite conducting cylinder of radius a as shown in Figure 2.11. Let (r, φ, z) be a system of cylindrical coordinates such that the z-axis coincides with the axis of the cylinder and the angle φ is measured from the direction of propagation of the incident wave. We assume that the time dependence is described by the factor $\exp(j\omega t)$, where ω is the angular frequency of the incident field, and that the electric field vector of the incident wave is parallel to the axis of the cylinder.

Then the problem reduces to finding the complex amplitude of the scattered field E satisfying Helmholtz's equation

$$\frac{1}{r}\frac{\partial}{\partial}\left(r\frac{\partial E}{\partial r}\right)+\frac{1}{r^2}\frac{\partial^2 E}{\partial \varphi^2}+k^2E=0 \tag{2.20}$$

and the boundary condition

$$E\Big|_{r=a}+E_0\exp(-jka\cos\varphi)=0 \tag{2.21}$$

The solution of our problem has the form

$$E=\sum_{n=0}^{\infty}N_n H_n^{(2)}(kr)\cos n\varphi \tag{2.22}$$

where the Hankel function is defined as $H_n^{(2)}(kr)=J_n(kr)-jY_n(kr)$.

The unknown coefficients can be evaluated by using the boundary condition and the following equality, which gives the incident field:

$$\exp(-jka\cos\varphi)=J_0(ka)+2\sum_{n=1}^{\infty}(-j)^n J_n(ka)\cos n\varphi \tag{2.23}$$

Therefore, the required solution for the scattered field is given by:

$$E = -E_0 \left[\frac{J_0(ka)}{H_0^{(2)}(ka)} H_0^{(2)}(kr) + 2\sum_{n=1}^{\infty} (-j)^n \frac{J_n(ka)}{H_n^{(2)}(ka)} H_n^{(2)}(kr) \cos n\varphi \right] \tag{2.24}$$

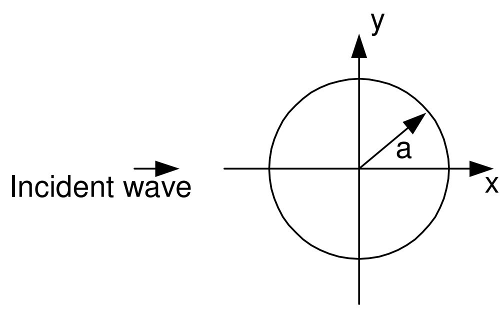

Figure 2.11 An incident plane wave in the presence of a PEC circular cylinder.

The series solution is exact in the sense that the series expansion yields the analytical solution for all frequencies. The ray-optical approach may be applied for the case where $2a >> \lambda$ as outlined below.

Let us denote the scattered field by u^s and the total field by u. The asymptotic theory is based on geometrical optics and the geometrical theory of diffraction [4-5]. In the asymptotic theory, one seeks the solution for u^s in $u = e^{-jkx} + u^s$, as a superposition of the form:

$$u^s(x,y) = \sum_{l=1}^{L} A_l(x,y) e^{jkS_l(x,y)} \tag{2.25}$$

Here L denotes the number of fields. In our specific example, the sum consists of a reflected field and possibly one or two diffracted fields, and a shadow forming field.

Each field $A(x,y)e^{jkS(x,y)}$ is a solution to the equation

$$\nabla u + k^2 u = 0 \tag{2.26}$$

where, A is called the amplitude, k is the wavenumber, $e^{jkS(x,y)}$ is the phase factor, and S is the phase. To determine the phase of each field we can use the methods of the asymptotic theory. First we substitute $A(x,y)e^{jkS(x,y)}$ into $\nabla u + k^2 u = 0$ and cancel the phase factor to obtain:

$$-k^2[(\nabla S)^2 - 1]A + 2ik\nabla S.\nabla A + ikA\nabla S + \nabla A = 0 \tag{2.27}$$

Equating the leading order term of equation (2.27), to zero, yields the eikonal equation of geometrical optics:

$$(\nabla S)^2 - 1 = 0\,. \tag{2.28}$$

This is a first order non-linear partial differential equation for the phase S, which we can solve by the method of characteristics. To do so, we introduce the two-parameter family of characteristic curves or rays $X(\sigma,\tau)$, $Y(\sigma,\tau)$ and the equations

$$\frac{dX(\sigma,\tau)}{d\sigma} = S_x, \quad \frac{dY(\sigma,\tau)}{d\sigma} = S_y. \tag{2.29}$$

In this case,

$$S_x \equiv S_x(\tau) \text{ and } S_y \equiv S_y(\tau) \tag{2.30}$$

are independent of the arc-length σ, because the index of refraction is a constant. Hence the rays propagate along straight lines in the direction ∇S

$$X(\sigma,\tau) = X(0,\tau) + \sigma S_x(\tau), \tag{2.31a}$$

$$Y(\sigma,\tau) = Y(0,\tau) + \sigma S_y(\tau) \tag{2.31b}$$

On each ray, the phase is determined from the equation

$$\frac{dS(\sigma,\tau)}{d\sigma} = 1 \tag{2.32}$$

$$S(\sigma,\tau) = S_0(\tau) + \sigma \tag{2.33}$$

The initial condition $S_0(\tau) = S|_\Gamma$ is determined on the surface of the scatterer $\Gamma(\tau)$:

$$\Gamma(\tau) = (X(0,\tau), Y(0,\tau)) \tag{2.34}$$

From the boundary condition

$$u^s = -e^{-jkx}, (x, y) \in \Gamma \tag{2.35}$$

for the reflected field,

$$S_0(\tau) = X(0,\tau) \tag{2.36}$$

Arguments pertaining to the geometrical theory of diffraction yield $S_0(\tau)$ for the diffracted fields.

To determine the ray direction $\nabla S_0(\tau)$ we use

$$(\nabla S)^2 - 1 = 0 \tag{2.37}$$

and the strip condition on Γ

$$\frac{dS_0(\tau)}{d\tau} = S_x(\tau)\frac{dX}{d\tau} + S_y(\tau)\frac{dY}{d\tau} \tag{2.38}$$

2.2.4.2 Rays of the Scattered Field

The scattered field consists of four terms

$$u_S = u_R + u_{sf} + u_{d+} + u_{d-} \ , \tag{2.39}$$

which are the reflected field u_R, the shadow forming field u_{sf}, the diffracted field u_{d+} originating at $(0,1)$, and the diffracted field u_{d-} originating at $(0,-1)$. The fields u_R and u_{sf} satisfy the boundary conditions

$$u_R(x,y) = -e^{-jkx} \quad (x,y) \in \Gamma \quad x < 0 \ , \tag{2.40}$$

$$u_{sf}(x,y) = -e^{-jkx} \quad (x,y) \in \Gamma \quad x \geq 0 \ . \tag{2.41}$$

Both diffracted fields vanish on the surface of the cylinder. The field u_{sf} in the region $x \geq 0$, $|y| \leq 1$ is called the shadow forming field because $u_{sf} + u_i$ vanishes in that region.

The rays

$$X(\sigma,\tau)=\cos\tau-\sigma\cos 2\tau \qquad \pi/2\le\tau\le 3\pi/2 \tag{2.42a}$$

$$Y(\sigma,\tau)=\sin\tau-\sigma\sin 2\tau \qquad \pi/2\le\tau\le 3\pi/2 \tag{2.42b}$$

are shown in the Figure 2.12 below.

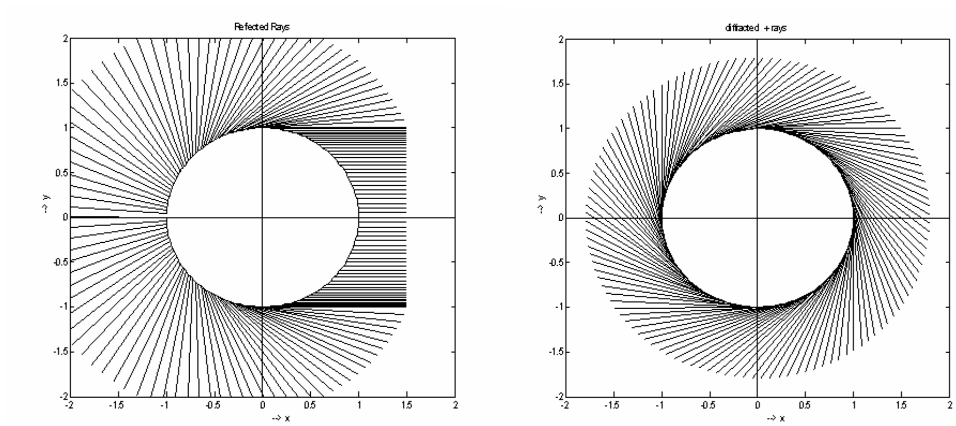

Figure 2.12 The figure on the left shows the rays reflected by the circular cylinder, and the rays of the shadow forming field. The figure on the right, shows the diffracted rays emanating from $(0,1)$.

For reflected rays, if we find out the angle, $\tau=\theta$, for each point, (x,y), in the suggested regions , we can determine corresponding reflected rays by using the equations given below:

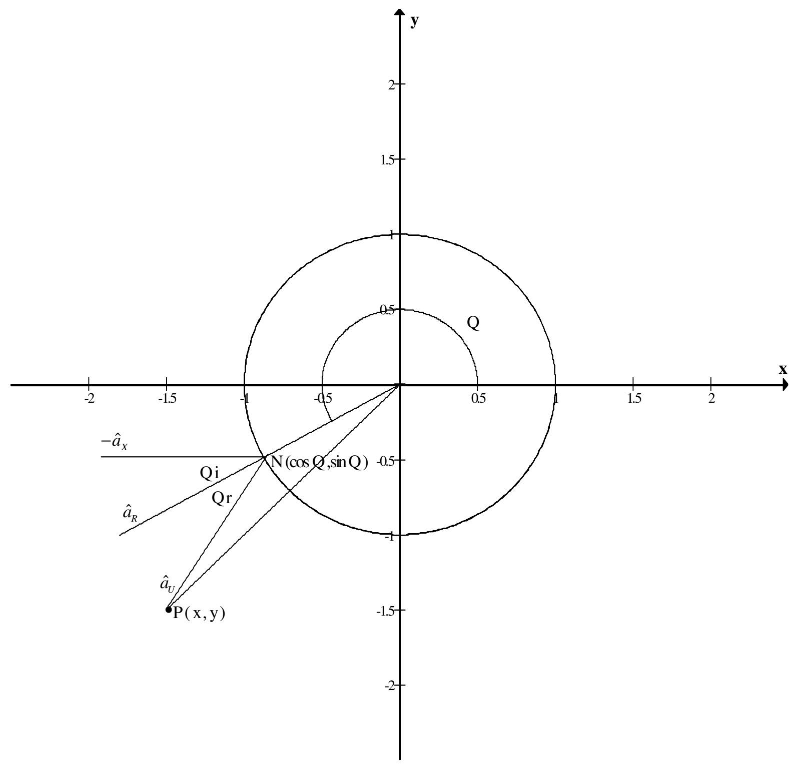

Figure 2.13 Geometrical explanation of the construction of reflected rays, where $\hat{a}_R$ is the unit reflected ray vector and $\hat{a}_U$ is the unit normal vector.

$$\hat{a}_U = \frac{\overline{P} - \overline{N}}{\left\| \overline{P} - \overline{N} \right\|}$$

$$= \frac{(x, y) - (\cos\theta, \sin\theta)}{\sigma}$$

$$= \frac{(x - \cos\theta, y - \sin\theta)}{\sigma}, \tag{2.43}$$

where

$$\sigma = \sqrt{x^2 - 2x\cos\theta + 1 + y^2 - 2y\sin\theta}$$

and

$$\hat{a}_R = (\cos\theta, \sin\theta) \ ,$$

then

$$\hat{a}_R \bullet \hat{a}_U = \frac{(\cos\theta, \sin\theta) \bullet (x - \cos\theta, y - \sin\theta)}{\sigma}$$

$$= \frac{\cos\theta(x - \cos\theta) + \sin\theta(y - \sin\theta)}{\sigma}$$

$$\hat{a}_R \bullet \hat{a}_U = \hat{a}_R \bullet (-\hat{a}_X)$$

$$= \frac{x\cos\theta + y\sin\theta - 1}{\sqrt{x^2 - 2x\cos\theta + 1 + y^2 - 2y\sin\theta}} = -\cos\theta$$

$$= \hat{a}_R \bullet (-\hat{a}_X) = -\cos\theta$$

$$f = x\cos\theta + y\sin\theta - 1 + \cos\theta\sqrt{x^2 - 2x\cos\theta + 1 + y^2 - 2y\sin\theta} = 0 \tag{2.44}$$

For a given point, (x, y), the angle θ can be found, by using f solve function of Matlab.

Similarly for u_{sf} the rays are

$$X(\sigma, \tau) = \cos\tau + \sigma \qquad -\pi/2 \le \tau \le \pi/2 \tag{2.45a}$$

$$Y(\sigma, \tau) = \sin\tau \qquad -\pi/2 \le \tau \le \pi/2 \tag{2.45b}$$

In the shadow region, $|y| \le 1$, $x > 0$, $u_{sf} + u_i$=0. However, the exact solution is nonzero there, in view of diffraction effects. The additional terms u_{d+} and u_{d-} account for the diffracted field. The rays associated with u_{d+} , u_{d-} are called diffracted rays. Each incident ray, which is tangent to the cylinder, gives rise to a surface diffracted ray. Here the incident rays are tangent at $(0,1)$ and $(0,-1)$ and bound the shadow region.

Each surface diffracted ray travels along the surface of the cylinder starting at the point of diffraction. As it travels along the surface, it sheds additional diffracted rays into the domain. These new rays leave the surface of the cylinder tangentially.

The surface diffracted ray emanating from $(0,1)$ travels in the clockwise direction along the surface of Γ and sheds the family of rays

$$X(\sigma,\tau) = \sin\tau + \sigma\cos\tau \qquad \tau,\sigma \geq 0 \tag{2.46a}$$

$$Y(\sigma,\tau) = \cos\tau - \sigma\sin\tau \tag{2.46b}$$

The surface ray emanating from $(0,-1)$ travels in the anticlockwise direction and sheds the family of diffracted rays

$$X(\sigma,\tau) = \sigma\cos\tau - \sin\tau \qquad \tau,\sigma \geq 0\ 2. \tag{2.47a}$$

$$Y(\sigma,\tau) = \sigma\sin\tau - \cos\tau \tag{2.47b}$$

For diffracted rays, if we find out the angle, $\tau = 90 - \theta$, for each point, (x, y), in the suggested regions, we can determine corresponding diffracted rays by using the equations given below:

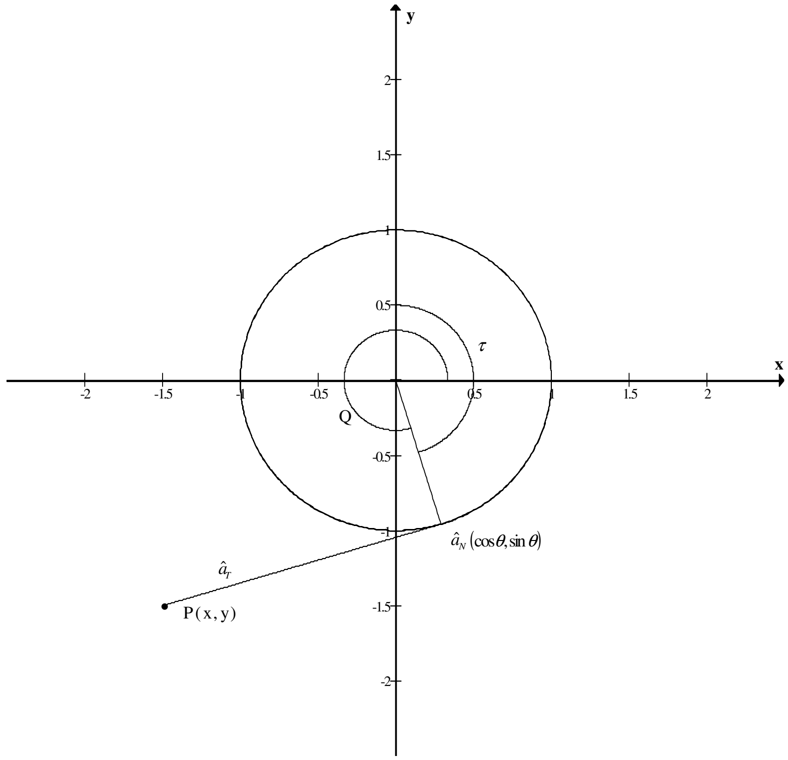

Figure 2.14 Geometrical explanation of the construction of diffracted rays, emanating from $(0,1)$ where $\hat{a}_T$ is the unit reflected ray vector and $\hat{a}_N$ is the unit normal vector.

$$\hat{a}_N \bullet \hat{a}_T = (\cos\theta, \sin\theta) \bullet \frac{(x - \cos\theta, y - \sin\theta)}{\sigma} \tag{2.48}$$

$$= \frac{\cos\theta(x - \cos\theta) + \sin\theta(y - \sin\theta)}{\sigma} = 0 \tag{2.49}$$

$$f = x\cos\theta_{1,2} + y\sin\theta_{1,2} - 1 = 0 \tag{2.50}$$

Therefore, for a given point, (x, y), the angles $\theta_{1,2}$ can be found, by using f solve function of Matlab.

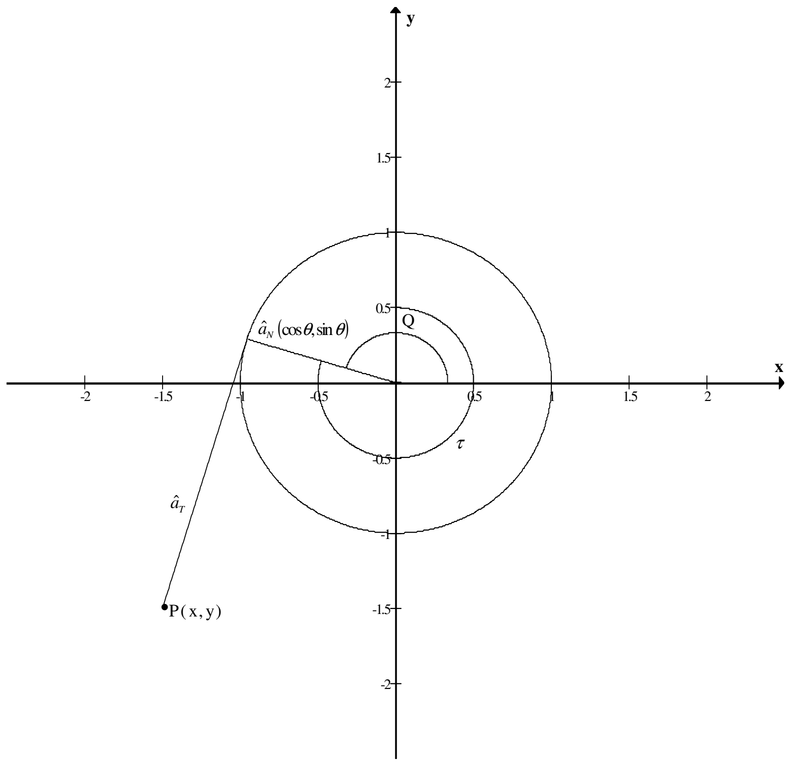

Figure 2.15 Geometrical explanation of the construction of diffracted rays, emanating from $(0,-1)$ where $\hat{a}_T$ is the unit reflected ray vector and $\hat{a}_N$ is the unit normal vector.

2.2.4.4 The Sommerfeld Half-plane Problem

The geometry of the Sommerfeld half-plane problem is given in Figure 2.16 below:

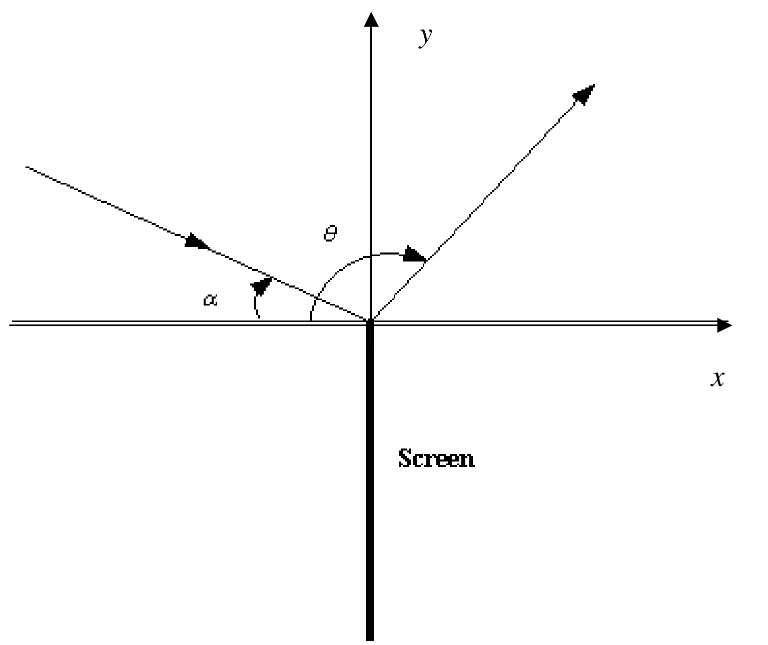

Figure 2.16 The geometry of the Sommerfeld half-plane problem.

The screen is a PEC object with zero thickness occupying the negative vertical axis (i.e. $x = 0, y \le 0$). general, the angles between the incident and diffracted rays and the normal to the screen are α and θ, respectively.

We assume that the incident field is a *TMz* plane wave given by the equation:

$$E_z^{inc}(x, y) = \exp(-jkx) \tag{2.51}$$

It is clear that the incident wave travels in $+x$ direction, which implies that $\alpha = 0$. Using geometric optics, the reflected field can be evaluated as:

$$E_z^{ref}(x,y) = -\exp(jkx) \tag{2.52}$$

in the quadrant $x \le 0$, $y \le 0$.

The edge-diffracted field is given by:

$$E_z^{d}(x,y) = D.g^{-1/2}.\exp(jkg) \tag{2.53}$$

where $g = \sqrt{x^2 + y^2}$ and the diffraction coefficient D is

$$D = -\frac{\exp(-jk\pi/4)}{2(2\pi k)^{1/2}}[\sec(\theta/2) + \csc(\theta/2)] \tag{2.54}$$

It is important to note that the diffracted field is defined everywhere (i.e. for all (x, y). The region $x \ge 0$ and $y \le 0$ **i**s the shadow region with the shadow forming field:

$$E_z^{sf}(x,y) = -\exp(-jkx) \tag{2.55}$$

In summary, the incident and diffracted fields are defined everywhere, and the reflected and shadow-forming fields are defined in the third ($x \le 0$, $y \le 0$) **a**nd fourth ($x \ge 0$, $y \le 0$) quadrants, respectively.

CHAPTER 3

UTILIZATION OF THE 2D WFT FOR THE IDENTIFICATION OF SCATTERING MECHANISMS

In this chapter, the applicability of the 2D WFT for the identification of the ray directions is demonstrated via the two specific examples discussed in the previous chapter. The analysis approach will be given in detail for the scattering problem where the scatterer is an infinite PEC cylinder with circular cross-section. In this problem the input is the incident field $\overline{E}^{i}$ and the output is the scattered field $\overline{E}^{s}$, which is also z-polarized (as the incident field $\overline{E}^{i}$) and can be expressed as a linear combination of Bessel functions.

$$\overline{E}^{i} = \hat{a}_z e^{-jkx} = \hat{a}_z e^{-jkr\cos\varnothing} = \hat{a}_z e^{-j\bar{k}.\bar{r}} \tag{3.1}$$

$$\overline{E}^{tot} = \overline{E}^{i} + \overline{E}^{s} \tag{3.2}$$

where

$$k = \left|\bar{k}\right| = \frac{\omega}{c} = \frac{2\pi f}{c} \tag{3.3}$$

The total field, $\overline{E}^{tot}$, is the sum of the incident and scattered fields and it satisfies the Helmholtz Equation, where the boundary conditions are:

$$\overline{E}^{tot} = 0 \text{ for } |\rho| < a$$

$$\overline{E}^{tot} = 0 \text{ at } \rho = a \tag{3.4}$$

Then, the resulting solution for the scattered field can be approximately expressed as a linear combination of cylindrical waves for $k\rho >> 1$. This is the large argument case for Hankel functions.

In order to check the validity for the large argument assumption, let $k = 32\pi$ be chosen in the simulations and $\rho = 1.5m$ Then,

$$k\rho = 32\pi \frac{3}{2} = 48\pi \tag{3.5}$$

$$k\rho \cong 151 >> 1 \tag{3.6}$$

The wavelength and frequency are evaluated as

$$k = \frac{w}{c} = \frac{2\pi f}{c} = \frac{2\pi}{\lambda} = 32\pi \;\; \lambda = 0.0625m. \tag{3.7}$$

and

$$f = \frac{c}{\lambda} = \frac{3\times10^8}{\frac{1}{16}} = 4.8GHz. \tag{3.8}$$

The scattered field can be expressed as the superposition of cylindrical waves as

$$\overline{E}^s = \hat{a}_z \sum_m \alpha m \frac{\exp\left(-jk\hat{u}_m.\overline{r}\right)}{\sqrt{k\rho}} \tag{3.9}$$

where the position vector $\overline{r}$ *is :*

$$\overline{r} = x\hat{a}_x + y\hat{a}_y = \rho\hat{a}\rho \tag{3.10}$$

and the wave number is

$$k = \left|\overline{k}\right| = \frac{2\pi f}{c} = \frac{2\pi}{\lambda} \tag{3.11}$$

where $\overline{k} = k\hat{u}_m = k\left(u_{mx}\hat{a}_x + u_{my}\hat{a}_y\right)$, α_m is a constant, and $\hat{u}_m$ is the unit vector in the direction of propagation of the m^{th} scattered component.

The above expression can be deduced from the large argument approximation for a v^{th} order 2^{nd} kind Hankel function:

$$H_{\gamma}^{(2)}(\zeta) \approx \sqrt{\frac{2}{\pi\zeta}\exp\left(-j\left(\zeta - \frac{1}{2}\gamma\pi - \frac{\pi}{4}\right)\right)} \tag{3.12}$$

In our case, $\zeta = k\rho$

Then,

$$\overline{E}^{S}(x, y) = \hat{a}_{z} \sum_{m} \beta m \frac{e^{-jk(xu_{mx}+yu_{my})}}{\sqrt{k}(x^{2}+y^{2})^{\frac{1}{4}}} \tag{3.13}$$

Let

$$g(\rho) = \frac{1}{\sqrt{k\rho}} \tag{3.14}$$

then z-component of the scattered field will be:

$$E_{z}^{S} = \sum_{m} \beta_{m} . g(\rho) \exp(-jk(xu_{mx} + yu_{my})) \tag{3.15}$$

where

$$\beta_m = \alpha_m \sqrt{\frac{2}{\pi}} e^{j\frac{1}{2}v\pi} e^{j\frac{\pi}{4}} \; . \tag{3.16}$$

$$FT\left\{E_x^s\right\} = \sum_m \beta m \;\; FT\left\{ g\left(\sqrt{x^2+y^2}\right) e^{-jk\left(Um_x x + Um_y y\right)} \right\} \tag{3.17}$$

where the 2-D Fourier Transform is defined as:

$$G(fx, fy) = \frac{1}{2\pi} \int_{-\infty}^{\infty}\!\!\int g(x', y')\, ej2\pi(x'fx + y'fy)\, dx'dy' \tag{3.18}$$

$$\mathrm{FT}\left\{ g(x, y)\, .e^{-jku_{mx}x} e^{-jku_{my}y} \right\} = G(f_x + \tfrac{U_{mx}}{\lambda}, f_y + \tfrac{U_{my}}{\lambda})) \tag{3.19}$$

where

$$ku_{mx} = -\tfrac{2\pi f}{c} u_{mx} = -2\pi \tfrac{u_{mx}}{\lambda} \quad \text{and} \quad ku_{my} = \tfrac{-2\pi f u_{my}}{c} = -2\pi \tfrac{u_{my}}{\lambda} \tag{3.20}$$

However, in this problem for instance, the basic scattering mechanisms are reflection and surface waves originating from $(x = 0, y = 1)$ and $(x = 0, y = -1)$ points. All these three scattering mechanisms lead to cylindrical waves (all z-polarized), whose propagation directions keep changing with respect to the observation points.

A simple 2-D FT cannot isolate these components as integrals in equations are computed over the ranges $(-\infty,+\infty)$.

Instead, the 2-D WFT must be computed over smaller regions in the x-y plane, chosen by the window function of the WFT [16].

$$\text{WFT } \left\{E_z^s\right\} = \sum_m \beta m \text{ WFT } \left\{g(\sqrt{x^2+y^2})e^{-jk(xu_{mx}+yu_{my})}\right\} \tag{3.21}$$

Assume that window of WFT is narrow enough to take $g(\sqrt{x^2+y^2}) = \frac{1}{\sqrt{k\rho}} \approx$ constant around the center point (x, y).

Then,

$$E_z^s(x, y, f_x, f_y) = \sum_m \beta m \iint_{x'y'} e^{-jk(x'u_{m_x}+y'u_{m_y})}\ W(x-x', y-y').$$
$$e^{-j2\pi(x'f_x+y'f_y)dx'dy'} \tag{3.22}$$

where $W(x-x', y-y')$ is a properly chosen window function centered around (x, y).

Let us further assume that the window function is separable in x, y coordinates as:

$$W(x-x', y-y') = W_x(x-x').W_y(y-y') \tag{3.23}$$

An example of a separable window function is the rectangular window function given below

$$W(x-x', y-y') = \begin{cases} 1 & |x-x'| \le L, |y-y'| \le L \\ 0 & elsewhere \end{cases} \tag{3.24}$$

In the expression of the scattered field variation,

$$\overline{E}^s = \hat{a}_z \sum_m \beta m \frac{e^{-jk\hat{u}_m \cdot \bar{r}}}{\sqrt{\rho}} \tag{3.25}$$

$\hat{u}_m$ denotes the unit vector in the propagation direction of the m^{th} scattered field component as

$$\hat{u}_m = U_{m_x} \hat{a}_x + U_{m_y} \hat{a}_y \tag{3.26}$$

E^s will asymptotically tend to a plane wave in the far field as

$$\overline{E}^{s} \cong \hat{a}_{z} \sum_{m} \beta m \; e^{-jk\hat{u}_{m}.\bar{r}} \tag{3.27}$$

Using the linearity of the WFT, we get

$$\text{WFT}\left\{E_{z}^{s}\right\} = \sum_{m} \beta m \; \text{WFT} \; \left\{e^{-jk(xu_{mx}+yu_{my})}\right\} \tag{3.28}$$

where $k = \frac{2\pi f}{c}$. The expression above can be written as

$$E_{z}^{s}(x, y, f_{x}, f_{y}) = \sum_{m} \beta m \iint_{x'y'} e^{-jk(x'u_{mx}+y'u_{my})} W(x'-x, y'-y) e^{-j2\pi(x'f_{x}+y'f_{y}dx'dy')}$$

(3.29)

where f_{x}, f_{y} are spatial frequencies, and $W(x-x', y-y')$ is a window function centered around the point x, y.

Then the scattered field will be:

$$E_{z}^{s}(x, y, f_{x}, f_{y}) = \sum_{m} \beta m \iint_{x'y'} W(x'-x, y'-y) e^{-j2\pi[x'(\frac{Umx}{\lambda}+f_{x})+y'(\frac{Umy}{\lambda}+f_{y})'} dx' dy'$$

$$=\sum_m \beta m \int_{x'} w_x(x'-x)e^{-j2\pi x'(\frac{Umx}{\lambda}+f_x)}\ dx' \int_{y'} Wy(y'-y)e^{-j2\pi y'(\frac{Umy}{\lambda}+f_y)} dy' \tag{3.30}$$

If the windows are infinitely large, (i.e. FT case), then:

$$\int_{x'} W_x(x'-x)\exp(-j2\pi x'(\tfrac{Umx}{\lambda}+f_x)_{dx'}) \approx \int_{-\infty}^{\infty} \exp(-j2\pi \tfrac{Umx}{\lambda} x')\ \ e^{-j2\pi x' fx} dx'$$

$$=2\pi\ \ \delta(w+2\pi \tfrac{Umx}{\lambda})$$

$$=\sum 2\pi\ \delta\ \ (2\pi f_x + 2\pi \tfrac{Umx}{\lambda}) \tag{3.31}$$

Note that $\delta\ \ (2\pi f_x + 2\pi \frac{Umx}{\lambda})$ is non-zero only at $f_x = -\frac{Umx}{\lambda}$

$$E_z^s(x,y,f_x,f_y) \approx \sum_m \beta m\ (2\pi)^2\ \ \delta(2\pi f_x + 2\pi \tfrac{Umx}{\lambda})\ \delta(2\pi f_y + 2\pi \tfrac{Umy}{\lambda})$$

(3.32)

is non-zero at $f_x = -\frac{Um_x}{\lambda} = -\frac{Umx}{2\pi}k$ and $f_y = -\frac{Umy}{\lambda} = -\frac{Umy}{2\pi}k$ where $\lambda = \dfrac{2\pi}{k}$.

In our specific applications the number of samples, is chosen as $N = 256$.

For extension in x-direction is taken as $X_o = 4$ (i.e. $-2 \le x \le 2$) which yields $\Delta f_x = \frac{1}{4}$, and maximum frequency $fx_{\max} = \frac{N}{2}\Delta fx = 32$.

Similarly the extension in y-direction is taken as $Y_o = 4$ (i.e. $-2 \le y \le 2$), $\Delta fy = \frac{1}{4}$, and maximum frequency $fy_{\max} = \frac{N}{2}\Delta fy = 32$.

Reading f_x and f_y from the WFT map, direction vectors, Umx and Umy can be found as:

$$Umx = -\frac{2\pi fx}{k} \quad \text{and } Umy = -\frac{2\pi fy}{k} \text{ where } \frac{Umy}{Umx} = \frac{fy}{fx}. \tag{3.33}$$

In the simulations, we chose

$$k\rho = 32\pi\frac{3}{2} = 48\pi \tag{3.34}$$

Therefore the wave number will be:

$$k = \frac{w}{c} = \frac{2\pi f}{c} = \frac{2\pi}{\lambda} = 32\pi \;\; \lambda = 0.0625m. \tag{3.35}$$

and the frequency will be

$$f = \frac{c}{\lambda} = \frac{3\times 10^{8}}{\frac{1}{16}} = 4.8GHz. \tag{3.36}$$

where the diameter of the cylinder is 2 meters.

Since the condition for the resonance region is $0.1 \le \frac{d}{\lambda} \le 10$. Then we can say that, we are in the near optical region, since $\frac{d}{\lambda} = \frac{2}{\frac{1}{16}} = 32.$

$$f_x^2 + f_y^2 = \tfrac{Umx^2}{4\pi} k^2 + \tfrac{Umy^2}{4\pi} k^2 = \tfrac{k^2}{4\pi^2}(u_{mx}{}^2 + u_{my}{}^2) \tag{3.37}$$

$$\sqrt{fx^2 + fy^2} = \tfrac{k}{2\pi} = \tfrac{32\pi}{2\pi} = 16 = \tfrac{1}{\lambda} \tag{3.38}$$

$u_{mx}{}^2 + u_{my}{}^2 = 1$ as $\hat{u}$ is a unit vector.

It is also straightforward to conclude that this analysis can be extended to the Sommerfeld Half-plane Problem to identify the ray directions at different space points.

The results for the scattering problem where the scatterer is an infinite PEC cylinder with circular cross-section, are shown in Figures 31.-3.22.

The spatial domain is a square $-2 \le x, y \le 2$, and the PEC cylinder occupies the region $x^2 + y^2 \le 1$. The wavenumber is $k = 32\pi$. The real part of the scattered field is shown in Figure 3.1, and the absolute value of its Fourier transform is given in Figure 3.2.

The non-zero components of the Fourier transform are located approximately on the circle with radius 32π, demonstrating the impossibility of the localization of the ray directions. In fact, all possible ray directions appear in the Fourier transform application due to the fact that the Fourier transform reflects the spectral properties of the function globally. Similar arguments hold for the total field and its Fourier transform shown in Figures 3.3. and 3.4. In Figures 3.5-3.22, the 2D WFT magnitude plots are given, where the window function center point moves on a circle of radius $1.5m$, and the window function is Gaussian with extension $1m$.

It is clear from these figures that, depending on the location of the center point, the ray directions corresponding to the reflected, surface diffracted or shadow forming fields are identified accurately via the WFT.

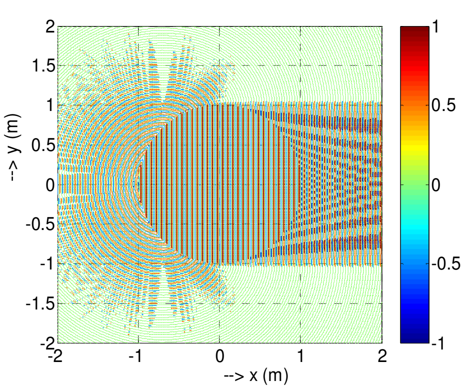

Figure 3.1 The real part of the scattered Field.

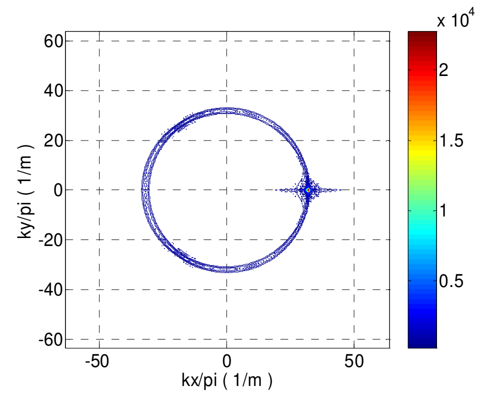

Figure 3.2 The absolute value of the Fourier transform of the scattered field.

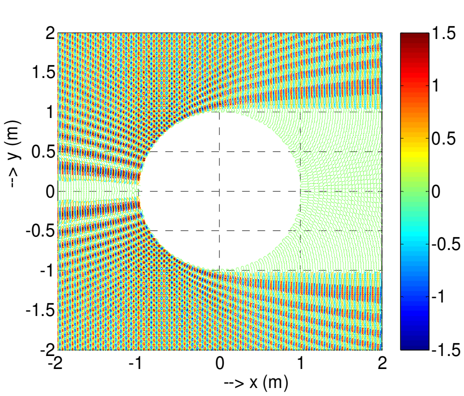

Figure 3.3 The real part of the total field

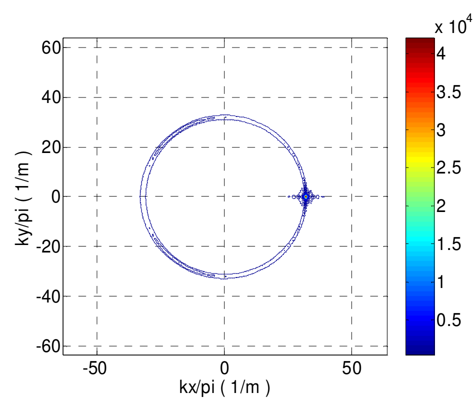

Figure 3.4 The absolute value of the Fourier transform of the total field

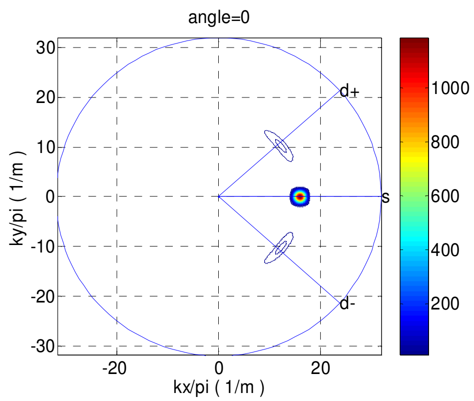

Figure 3.5 2D WFT of the scattered field with window center at x=1.500, y= 0.000.

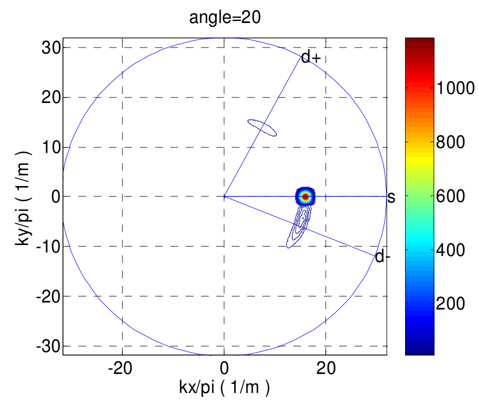

Figure 3.6 2D WFT of the scattered field with window center at x= 1.410, y= 0.513.

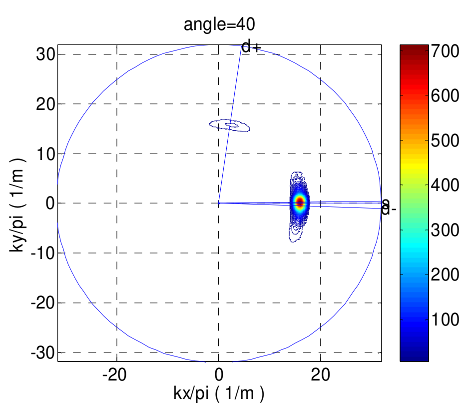

Figure 3.7 2D WFT of the scattered field with window center at x= 1.149, y= 0.964.

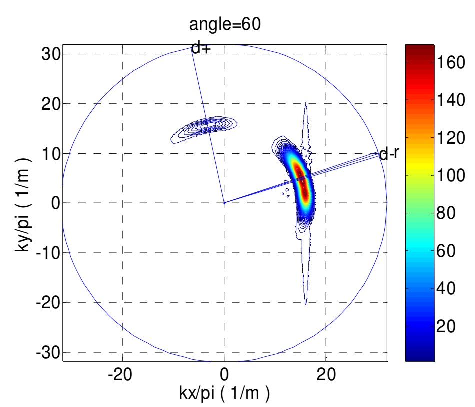

Figure 3.8 2D WFT of the scattered field with window center at x= 0.750, y= 1.299.

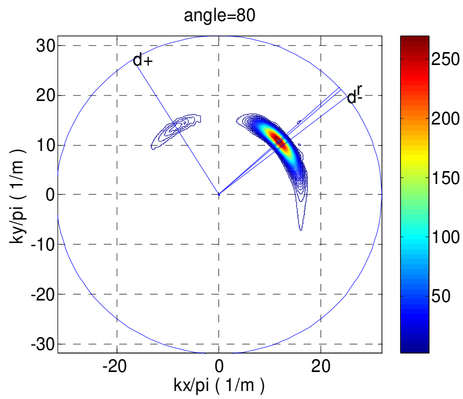

Figure 3.9 2D WFT of the scattered field with window center at x= 0.261, y= 1.477.

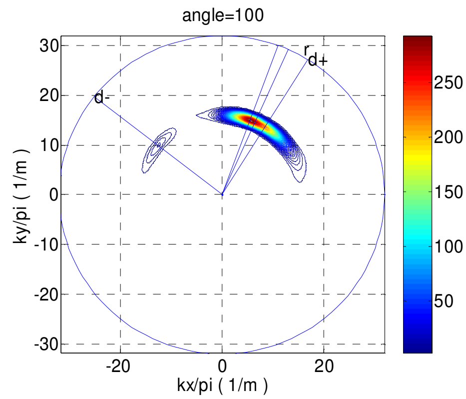

Figure 3.10 2D WFT of the scattered field with window center at x= -0.261, y= 1.477.

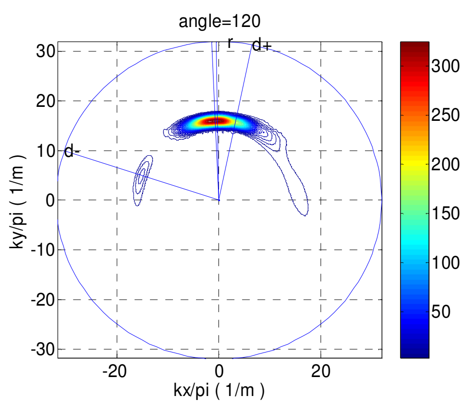

Figure 3.11 2D WFT of the scattered field with window center at x= -0.750, y= 1.299.

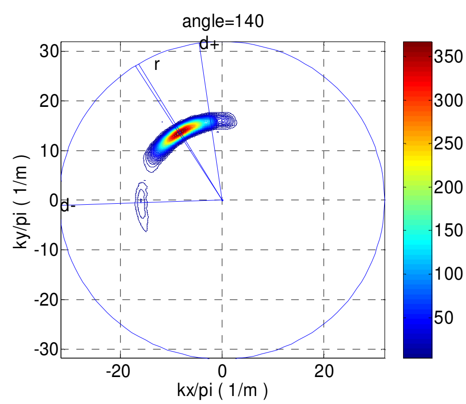

Figure 3.12 2D WFT of the scattered field with window center at x=-1.149, y= 0.964.

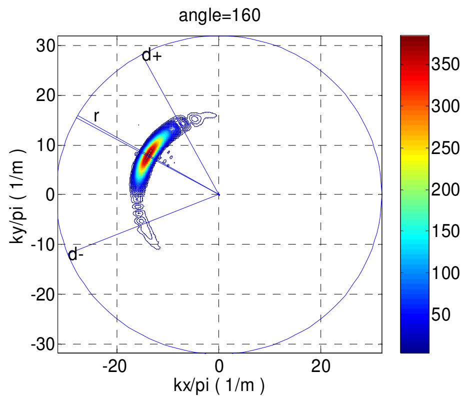

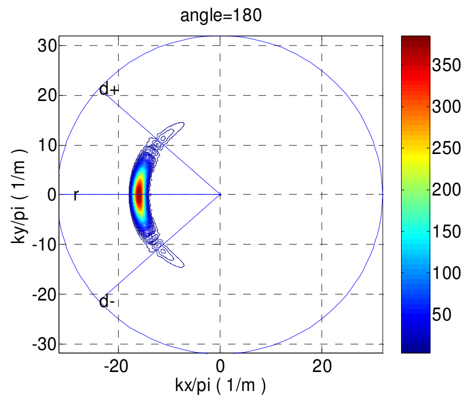

Figure3.13 2D WFT of the scatered field with window center at x= -1.409, y= 0.513.

Figure 3.14 2D WFT of the scattered field with window center at x=-1.500, y= 0.000.

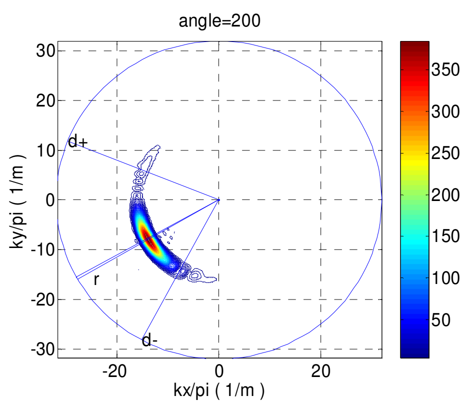

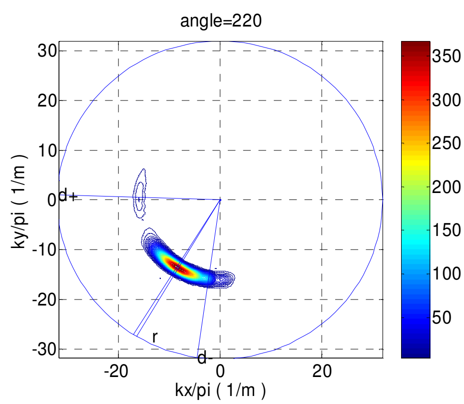

Figure 3.15 2D WFT of the scattered field with window center at x=-1.410, y=-0.513.

Figure 3.16 2D WFT of the scattered field with window center at x=-1.149, y=-0.964

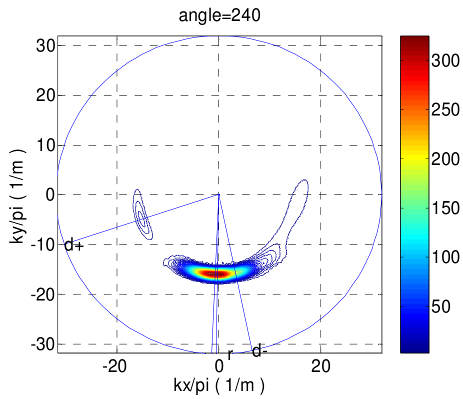

Figure 3.17 2D WFT of the scattered field with window center at x=-0.750, y=-1.

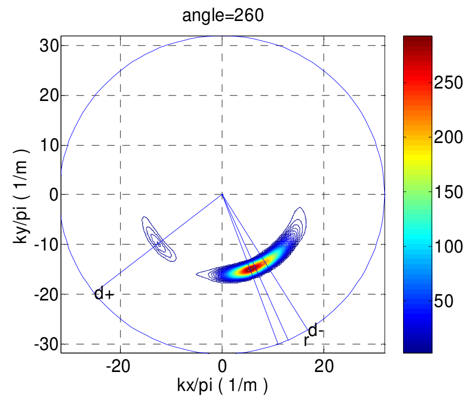

Figure 3.18 2D WFT of the scattered field with window center at x=-0.261, y=-1.477.

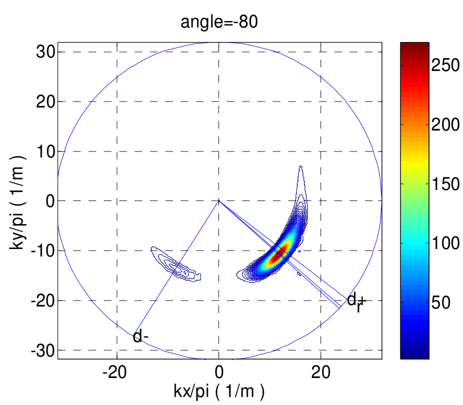

Figure 3.19 2D WFT of the scattered field with window center at x=0.261, y=-1.477.

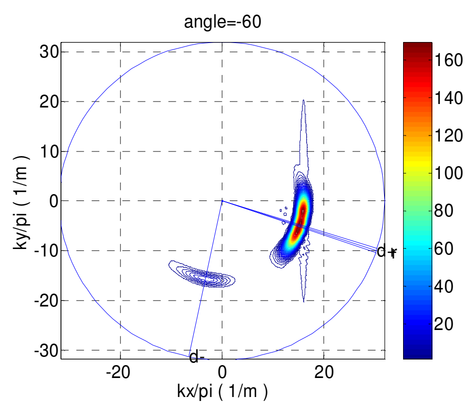

Figure 3.20 2D WFT of the scattered field with window center at x= 0.750, y=-1.299.

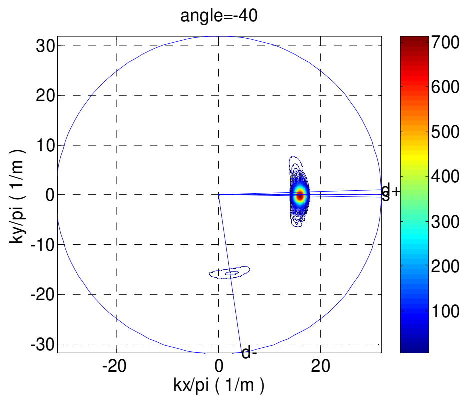

Figure 3.21 2D WFT of the scattered field with window center at x= 1.149, y= -0.964.

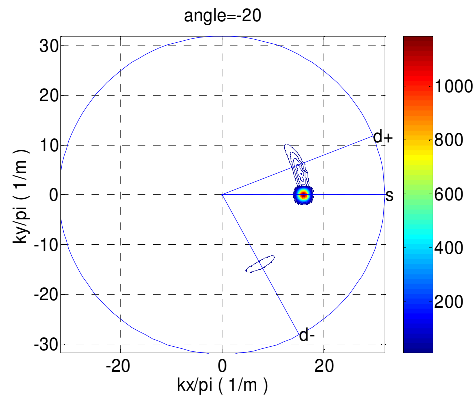

Figure 3.22 2D WFT of the scattered field with window center at x= 1.410, y= -0.513.

The results for the Sommerfeld half-plane problem also demonstrate the effectiveness of the WFT in the identification of different scattering mechanisms. The wavenumber is again chosen as $k = 32\pi$.

The 2D WFT magnitude plots are given in Figures 3.23-3.26, by choosing the center points of the Gaussian window function (with extension $1m$) as the centers of the four quadrants of the square spatial domain.

It is clear from the results that the WFT is able to identify the different ray components successfully.

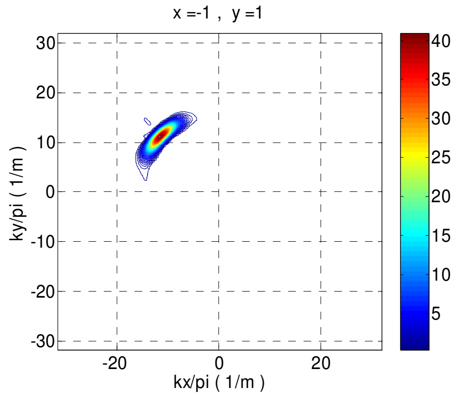

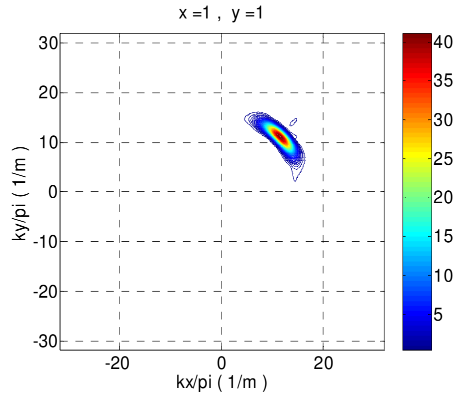

Figure 3.23 The real part of the scattered field Figure.

Figure 3.24 The absolute value of the Fourier transform of the scattered field Figure.

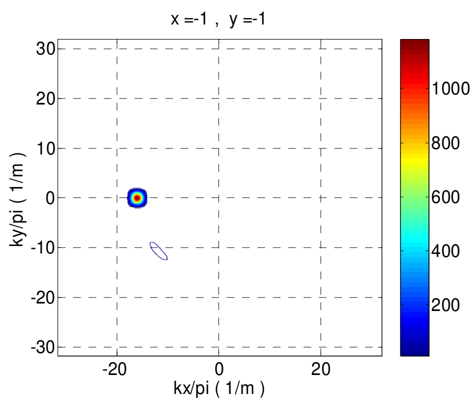

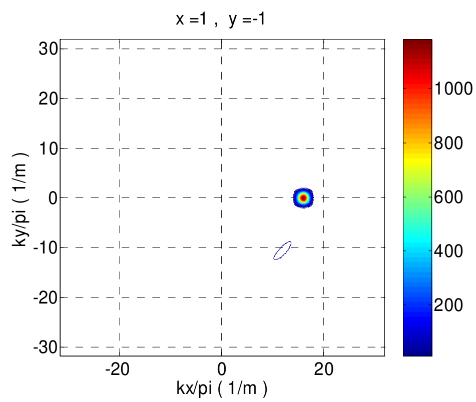

Figure 3.25 The real part of the total field Figure.

Figure 3.26 The absolute value of the Fourier transform of the scattered field.

CHAPTER 4

CONCLUSIONS

In this thesis the WFT has been used for the local spectral analysis of scattered electromagnetic field variations. It has been demonstrated that, the local field variation can be represented as a superposition of rays in high frequency scattering problems and the ray directions can be extracted by means of the WFT.

The theoretical justification of the approach is explained in detail in Chapter 2, by demonstrating that the ray directions may be obtained by using the plots of the WFT of the scattered field. The validity of the approach is shown in two specific examples which have analytical solutions with relatively easy ray-optical analysis. In the PEC circular cylinder scattering problem, the rays corresponding to the reflected, surface diffracted, and shadow-forming fields can be easily identified. Similarly, in the Sommerfeld half-plane problem, the ray directions corresponding to the reflected, edge-diffracted and shadow-forming fields can be found at any space point by means of simple geometric reasoning. In these examples, the WFT approach successfully identified the ray directions of the components of the scattered field.

It is important to notice that the spatial localization provided by the WFT is crucial in the identification of the ray directions. This information cannot be extracted from the Fourier transform, since the Fourier transform yields the global spectral characteristics of a function. It is clear from the examples in Chapter 3 that the Fourier transform yields all possible ray directions, which is not a very useful information. The local ray directions are achievable by the WFT through the spectral analysis of the localized spatial function.

The results related to the specific applications have been obtained by user-friendly MATLAB codes with graphic outputs for the visualization of the relationship between the WFT intensity and ray directions. These results clearly demonstrate the applicability of this method to identify the ray directions in scattering applications.

One of the potential applications of this approach is to use the identified ray directions in ray tracing. In this way it may be possible to trace the rays back to the points where they emerge. This information may be used in object recognition to extract the geometry of the scatterer.

REFERENCES

[1] E. Giladi, and J. B. Keller, A Hybrid Numerical Asymptotic Method for Scattering Problems, J. Compu. Phy. vo1. 74, pp. 226-247, 2001.

[2] L. Cohen, Time-Frequency Analysis, Prentice Hall, Englewood Cliffs, New Jersey, 1995.

[3] J. B. Keller, Geometrical theory of diffraction, J. Opt. Soc. Am. 52, 116 1962.

[4] J. B. Keller, Diffraction by a convex cylinder, Trans. IRE AP-4, 312,1956E.

[5] Zauderer, Partial Differential Equations of Applied Mathematics, Wiley-Interscience, New York, 1989.

[6] R. N. Bracewell, The Fourier Transform and Its Applications, Third Edition.

[7] S. Qian and D. Chen, Joint Time-Frequency Analysis: Methods and Applications, NJ: Prentice Hall, 1996.

[8] L. Cohen, Time-Frequency Distributions-A review, Proceedings of IEEE, vol. 77, pp. 941-979, 1989.

[9] F. Hlawatsch and F. Boudreaux-Bartels, Linear and Quadratic Time-Frequency Signal Representations, IEEE SP Magazine, pp. 21-67, 1992.

[10] D. Gabor, Theory of Communications, J.IEE, vol. 93, no. III, pp. 429-457, November 1946.

[11] A. Ishimaru, Electromagnetic Wave Propagation, Radiation, and Scattering, Prentice-Hall, 1991.

[12] K. Kunz, and R. Luebbers, The Finite Difference Time Domain for Electromagnetics, CRC Press, 1993.

[13] R.F. Harrington, Field Computation by Moment Methods, New York:Mavmillan,1968.

[14] J. N. Reddy, Introduction to the Finite Element Method, McGraw-Hill, 01 January, 1993.

[15] J.A. Kong, Electromagnetic Wave Theory, New York: Wiley,1986.

[16] G. T. Sayan, unpublished notes.